ELSEVIER

Computation of ac responses of arbitrary electrode geometries from the corresponding secondary current distributions: A method based on analytic continuation

Bosco Emmanuel [*],[1]

Modeling and Simulation Group, Central Electrochemical Research Institute, Karaikudi, India

Abstract

A method of analytic continuation is advanced for computing ac responses of electrochemical systems with arbitrary electrode geometries and proposed as an exact alternative to the approximate and intuitive transmission line models (TLMs). Using a complex extension of the boundary element method, the small signal ac responses were computed for several Hull cell geometries, the rectangular pore, the saw-tooth and a fractal geometry. A comparison with the results of the TLMs for the rectangular pore and the saw-tooth reveal quantitative as well as qualitative differences. Besides providing a bench-mark for such approximate theories, the present method may well be the only option for system geometries not amenable to a TLM. An alternative approach to the study of the constant phase element based on analytic continuation is also sketched.
© 2007 Elsevier B.V. All rights reserved.

Keywords: AC impedance; Current distribution; Analytic continuation; Hull cells; Fractal electrodes; Constant phase elements

1. Introduction

Current–potential distribution and the ac response of electrochemical systems are two important areas of Electrochemistry and Electrochemical Engineering. The geometry of the electrochemical system influences both the current–potential distribution and the ac impedance response. When we solve the distribution problem, say by using the Laplace equation, the geometry of the system enters explicitly along with the boundary conditions to be satisfied on the boundaries. In contrast, when we solve the impedance problem on non-trivial geometries, such as the cylindrical pore and the saw-tooth geometry, one usually invokes the transmission line model [1] with some physical/geometric approximation for the model parameters. The transmission line model (TLM) is an interesting

model pioneered by de Levie. It has an intuitive appeal and been subjected to good and extensive use by electrochemists. Even fractal electrode surfaces have been modeled using the TLM, besides a host of simpler geometries [2–6]. However, as pointed out by de Levie himself and re-emphasized recently in [5], "the most important weakness in the TLM is the assumption that the current distribution is normal to the macroscopic surface that is a neglect of the true current distribution. For a rough surface, the lines of electric force do not converge evenly on the surface. The double layer will therefore be changed unevenly . . ." The tangential components of the interface charging were recognized by Scheider [3] and included in a branched TLM; however, the model is still qualitative. Another limitation of TLM must also be mentioned, namely the physical and geometrical approximation which enters the estimation of the TLM model parameters.

The primary question which we address in this paper is whether we can compute the exact ac impedance of electrochemical systems having arbitrary geometry, without

[*] Tel.: +91 04565 228986.
  E-mail address: boscoemmanuel@yahoo.co.in
[1] Member, American Chemical Society.

recourse to the transmission line model. We show that this is possible using "analytic continuation". More specifically, given a system and its current distribution, say as a solution of the Laplace equation with appropriate boundary conditions, we can deduce the ac response of the same system solely from the solution to the current distribution problem by applying analytic continuation either to the exact or approximate solution or to the numerical solution method.

In Section 2, this method of analytic continuation is briefly sketched and illustrated, for its pedagogical value, with the help of two otherwise most trivial problems: that of 1-D and the concentric cylinder electrodes. In Section 3 we describe the boundary element method (BEM) and it is applied to Hull cell geometries in Section 4 and to fractal geometry (a triadic Cantor bar electrode) in Section 5. For Hull cells, fractals and a host of other geometries, no analytic solution is of course available even for the secondary current distribution from which to obtain the ac impedance by analytic continuation. Hence, it was found necessary to incorporate the "analytic continuation" in the numerical solution method itself. This was done within the frame work of the boundary element method. Essentially, we used a complex extension of the BEM. In Section 6 we compare the predictions of the present method with those of the TLM for the rectangular pore and the saw-tooth geometry and Section 7 outlines an alternative approach to the constant phase element using analytic continuation. Section 8 has summary and concluding remarks.

2. The method of analytic continuation

To be specific, consider the secondary current distribution problem (sketched in Fig. 1) involving a medium of conductivity κ enclosed between two electrode boundaries B1 and B2. The differential equation to be solved for variable conductivity is

$$\nabla \cdot (\kappa \nabla \phi) = 0 \tag{1}$$

which reduces to the standard Laplace equation

$$\nabla^2 \phi = 0 \tag{2}$$
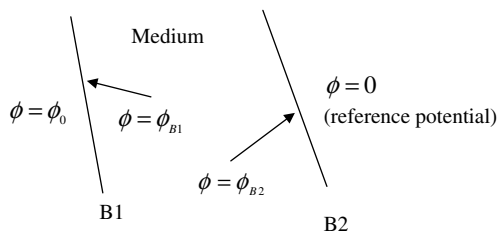
when κ is uniform in space.

Fig. 1. A 2-electrode system, defining the different potentials. B1 is the working electrode and B2 the counter-electrode.

As we are interested in relating the current distribution to the small signal ac response, we consider the linear polarization at the boundaries. For example, the boundary condition at the boundary B1 is

$$\kappa \nabla \phi \quad \text{at B1} = \frac{\phi_{B1} - \phi_0}{R_{ct,1}} \tag{3}$$

where ϕ_0 and ϕ_{B1} are respectively the potentials at the electrode side and electrolyte side of the electrode boundary B1 which may be taken as the working electrode. $R_{ct,1}$ is the charge-transfer resistance at B1. In general a similar condition may be applied at B2. However, for the purposes of this present work and without loss of generality, we take B2 as a counter electrode with zero charge-transfer resistance (i.e., a perfectly leaky capacitor) and consequently its role is restricted to its geometrical influence on the current distribution. By the same token, this leaky capacitor cannot hold any charge and hence does not affect the ac response either. We set $\phi_{B2} = 0$. However, we must keep in mind that for systems where both the electrodes influence the response, as for example in an electro-refining cell, one will have to maintain boundary conditions similar to Eq. (3) at both the electrodes.

Now we shall suppose that we have solved the Laplace equation (2) with the above boundary conditions at B1 and B2 and insulating boundary conditions at the remaining boundaries. If $\phi(x, y, z; \kappa R_{ct,1}, \text{etc.})$ is the exact (or approximate) analytical solution to this problem, the analytic continuation consists in replacing the simple charge-transfer resistance $R_{ct,1}$ at the boundary B1 by the complex interfacial impedance Z_1 at the same boundary. In conventional electrochemical systems, the medium conductivity κ is usually taken as real (i.e., purely resistive). However, κ is known to be complex for some media (the reader may consult the recent book by Barsoukov et al. [5] for several examples); solid media, with grains and grain–boundaries, are an important class where κ is complex. In such cases, we must of course do the analytic continuation in κ also, besides $R_{ct,1}$. Essentially, one takes a real current–potential distribution, analytically continue it to obtain the complex current–potential distribution having the phase information at each point of the 3-D space. In the simplest case the complexity enters through the boundary conditions and in the general case it may enter through the complex response of the medium also.

The above prescription for analytically continuing the dc current–potential distribution is easily established by discretising the medium and the boundaries into discrete volume and surface elements and applying Kirchoff's law to the resulting network (This network is an exact analogue of the physical system and is no way connected with the transmission line model. Nor does it involve the use of any lumped model parameters which the TLM does). Such an analysis leads to the following expression for the ac admittance of the system:

$$Y = \frac{\int_{B1} \kappa \nabla \phi \, dB1}{\phi_0} \tag{4}$$

where ϕ is the analytical continuation of the potential distribution and hence is now complex. Note further that, interestingly, ϕ_0 in Fig. 1 turns out to be the amplitude of the applied ac signal.

Two simple illustrations of the method are given below.

2.1. The case of 1-D

$$\frac{\partial^2 \phi}{\partial x^2} = 0 \tag{5}$$

$$-\kappa \frac{\partial \phi}{\partial x} = \frac{\phi_0 - \phi}{R_{ct1}} \quad \text{at } x = 0 \tag{6}$$

$$-\kappa \frac{\partial \phi}{\partial x} = \frac{\phi}{R_{ct2}} \quad \text{at } x = L \tag{7}$$

This system is trivially solved to obtain the potential and current distribution.

$$\phi = \phi_0 + \phi_0 \frac{(x + \kappa R_{ct1})}{(\kappa R_{ct1} + \kappa R_{ct2} + L)} \tag{8}$$

$$-\kappa \nabla \phi|_{B1} = i = -\frac{\phi_0}{R_{ct1} + R_{ct2} + (L/\kappa)} \tag{9}$$

where i is the current density.

Replace, in Eqs. (8) and (9), R_{ct1} and R_{ct2} by Z_1 and Z_2, the corresponding interfacial impedances; we obtain the complex potential and current. Now, the admittance follows from Eqs. (4) and (9) as

$$Y = \frac{A}{Z_1 + Z_2 + (L/\kappa)} \tag{10}$$

the expected result. A is the area of the electrode.

2.2. Concentric cylinder electrodes

$$\frac{\partial^2 \phi}{\partial r^2} + \frac{1}{r} \frac{\partial \phi}{\partial r} = 0 \tag{11}$$

$$-\kappa \frac{\partial \phi}{\partial r}\Big|_{r=b} = \frac{\phi(b) - \phi_0}{R_{ctb}} \tag{12}$$

$$\phi(a) = 0 \tag{13}$$

Solving this system, we obtain the following potential and current distribution:

$$\phi(r) = \frac{\phi_0}{\left\{\ln(b/a) + \frac{\kappa}{b} \cdot R_{ctb}\right\}} \cdot \ln\left(\frac{r}{a}\right) \tag{14}$$

$$i = -\kappa \frac{\phi_0}{r\left\{\ln(b/a) + \frac{\kappa}{b} R_{ctb}\right\}} \tag{15}$$

The analytic continuation $R_{ctb} \to Z_b$ gives the complex potential and current distributions. The system admittance is:

$$Y = \frac{A}{\left\{Z_b + \frac{b}{\kappa} \ln(b/a)\right\}} \tag{16}$$

where A is the area and Z_b the interfacial impedance of the outer electrode (Fig. 2).
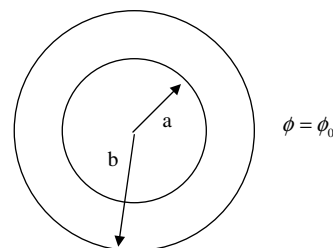

Fig. 2. Two concentric cylinder electrodes, of radii a and b and with the outer electrode kept at potential ϕ_0 with respect to the inner electrode.

3. The boundary element method and analytic continuation

For primary current distributions in two dimensions, some analytic solutions are possible by using conformal transformation. However, we cannot perform any non-trivial analytic continuation on a primary current distribution.[2] We need at least the secondary current distribution. Analytic solutions are hard to obtain for the secondary current distribution on non-trivial geometries even in 2-D. Numerical solutions are not an option, as we cannot analytically continue a numerical solution. Hence, the only option is to incorporate the analytic continuation in the numerical solution method itself.

In this section, we summarize and adopt the boundary element method for the numerical solution and embed analytic continuation. Essentially, it is a complex extension of the BEM. The use of the boundary element method [7], a cousin of the finite element method, is not new to Electrochemistry or Electrochemical Engineering. In particular, it has been used to compute the current–potential distributions for several cathodic protection problems [8–11] (in the area of corrosion), including its application by the present author to the cathodic protection of some really complex off-shore structures in the Arabian Sea [10,11]. The mathematical details of the boundary element method, pioneered by Brebbia [7], are well documented in the literature to which we refer the interested reader [7,12,13]. Omitting the mathematical details, we describe only the salient features of BEM relevant for our present context. BEM essentially involves a transformation (using the Green–Gauss Theorem) of the given partial differential equation (PDE), together with the boundary conditions, into an integral equation defined over the boundary of the system. When the boundary is discretised into the so-called boundary elements, this integral equation becomes a matrix–vector equation to be solved for the unknown variables (potentials and currents in our case) on the boundary. Though, for most purposes in Electrochemistry, one needs to know only the boundary potentials and currents, it is only a small additional step for BEM to compute the potentials and

---

[2] Of course, one can trivially perform an analytic continuation on a primary current distribution if the electrolyte conductivity is complex for some reason.

currents at any point in the bulk of the medium. Fig. 3 shows a typical Hull cell geometry with the boundary discretised into a number of boundary elements (N). The simultaneous equations to which the boundary element method eventually reduces is the following:

$$\sum_{j=1}^{N} L_{ij}P_j - \sum_{j=1}^{N} H_{ij}\phi_j = 0 \tag{17}$$

with i running from 1 to N. ϕ_j and P_j are respectively the potential and the normal gradient of the potential (related to the current $I_j = -\kappa P_j$) at the jth boundary element. L_{ij}'s and H_{ij}'s are the boundary element integrals which incorporate the Green's function of the PDE (the Laplace equation in our case) and also the system boundary information. The boundary conditions are not yet included. Typically we encounter, in the present work, any one of the following three types of boundary conditions on the jth element:

Dirichlet's condition: ϕ_j = a given value   (18)

Neuman's condition: P_j = a given value   (19)

$\qquad\qquad\qquad\qquad$ = 0 for insulating boundary elements

Robin's condition: $P_j = -\dfrac{1}{\kappa \cdot R_{ct}}(\phi_j - \phi_0)$ $\qquad$ (20)

for boundary elements subject to linear polarization.

Next we simply substitute these boundary conditions in the system of equations (17) and re-arrange the terms so that we end up with the following ($N \times N$, N) matrix–vector equation:

$$AX = R \tag{21}$$

with the vector X containing only the unknowns and the matrix A and the vector R containing only the knowns. This re-arrangement is known as the "assembly process" in the BEM literature. The vector X has the unknown potential (ϕ_j) or the unknown gradient (P_j), depending on the type of boundary condition applied to the jth element, for each of the N boundary elements.

In the conventional current–potential distribution problem, the elements of the matrix A and the vector R are all real. However when we perform analytic continuation by replacing R_{ct} (in the Robin's boundary condition) by the interfacial impedance Z_{int}, some of the elements of A and

R become complex. So we will be essentially solving a complex extension of the matrix vector equation (21), with complex algebraic operations replacing real algebraic operations. Consequently, the solution vector X will turn out to have complex elements representing the complex potentials and currents on the boundary elements. The admittance of the system follows easily as

$$Y = \left(\sum_j I_j\right) \Big/ \phi_0 \tag{22}$$

where I_j is the complex current normal to the jth boundary element and the summation runs over the boundary elements on the working electrode (or on the counter electrode; the equality of the two,[3] in the real and imaginary parts separately, provides a good check on the whole complex calculation).

4. Application to Hull cells

In this section, we apply the method outlined in the previous section to several Hull cell geometries and compute the Nyquist plots for a purely capacitive working electrode (Fig. 4a–d) and for a working electrode with a charge-transfer resistance in parallel i.e., a Voigt element (Fig. 5a–d). The dimensions of the Hull cell geometries, the double layer, the charge-transfer and the conductivity parameters are given for each plot. For the purely capacitive working electrode, there is a characteristic frequency dispersion for inclinations of the working electrode other than the vertical: there is a well-defined high frequency intercept on the real axis followed by a nearly linear regime which asymptotically tends to the classical vertical line. For the rectangular cell (Fig. 4d), one of course recovers the vertical line. When the working electrode is represented by a Voigt element, the classical semi-circle is recovered for the rectangular cell (Fig. 5d) whereas for the inclined geometries only distorted semi-circles result and the dispersion is such that the length of intersection on the real axis is much smaller than the charge-transfer resistance. For example, in Fig. 5c, the 'diameter' of the distorted semi-circle is 120 Ω instead 250 Ω for the rectangular cell.

Note further that the high frequency intercept on the real axis for any Nyquist plot in Fig. 4a–d is the same as the high frequency intercept in the corresponding Nyquist plot in Fig. 5a–d. Though this effective electrolyte resistance is a function of both the geometry and the frequency, the Nyquist plots in Fig. 4 show that there are clearly defined effective electrolyte resistances for the high and low frequency limits: the intercept on the real axis and the position of the vertical asymptote, respectively. However, for the conventional rectangular cell (see Fig. 4d), there is virtually no frequency dependence of the real part of the impedance with the high and low frequency limits of the effective electrolyte resistance coinciding. Hence, for the
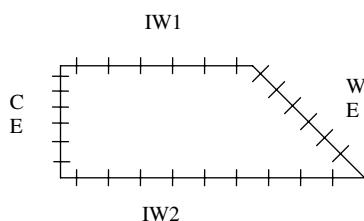

Fig. 3. A Hull cell showing the boundary elements. WE: working electrode, CE: counter electrode and IW1, IW2 are insulating walls. Further notations used in this paper: l_1 = length of IW1, l_2 = length of IW2 and l_3 = length of CE. Length of WE is fixed by l_1, l_2 and l_3.

_____

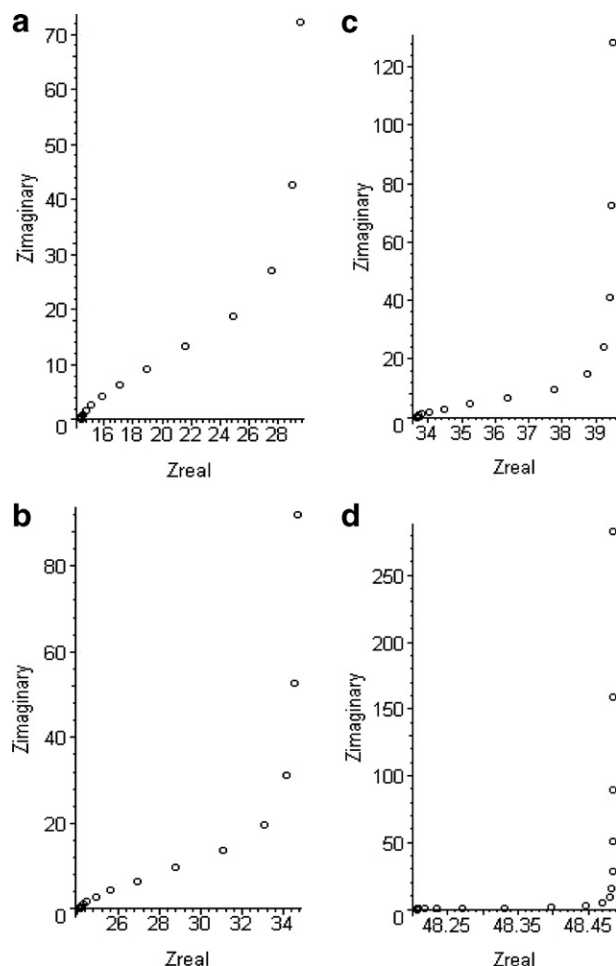[3] Except for the sign, which should be different.

Fig. 4. Nyquist plots for several Hull cell geometries. WE exhibits pure capacitive behavior. Electrolyte conductivity = 0.1 S/cm and double-layer capacity = 20 µF/cm^2. $l_2 = 5$ cm and $l_3 = 1$ cm for all the four geometrics. $l_1 = 1$ cm (a), 2 cm (b), 3 cm (c) and 5 cm (d). See caption to Fig. 3 for the meaning of l_1, l_2 and l_3.
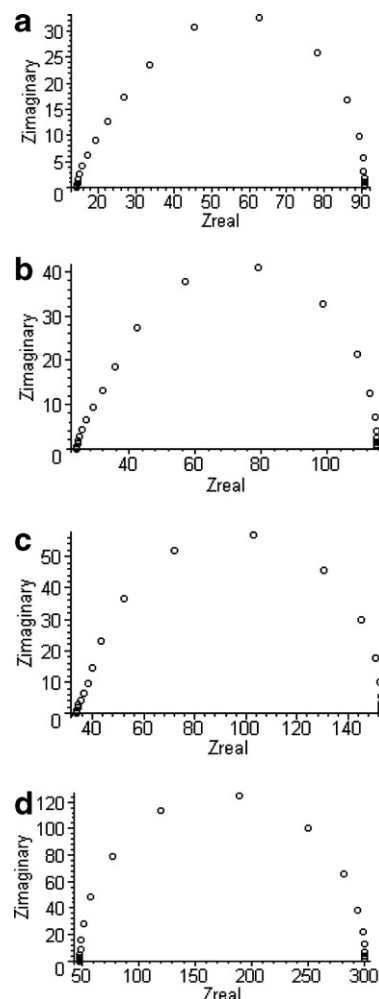

Fig. 5. Same as Fig. 4, except that the working electrode now exhibits linear charge-transfer polarization in parallel with capacitive charging. Charge-transfer resistance = 250 Ω cm^2.

rectangular geometry alone, this electrolyte resistance is given by the simple formula:

$$R = l/\kappa \cdot a$$

where l is the length and a the area of cross-section of the rectangular cell. For any other Hull Cell geometry, we need to compute the high and low frequency limits of this resistance by solving the Laplace equation in the complex domain as it is done in this paper.

Needless to say, a great practical advantage of our present method is that it computes, at one strike, the current distribution, effective solution resistances and the ac impedance of electrochemical systems of arbitrary geometry.

5. Application to a fractal electrode

As a further example of the method proposed here for computing the ac responses of arbitrary geometries, we study a triadic Cantor bar earlier investigated by Liu [2] in the context of the constant phase element (CPE). Liu

[2] and Scheider [3] used transmission line models to probe the CPE behavior. While Liu approximated the Cantor bar using a TLM, Scheider never identified the electrode geometry which corresponds to his TLM.

Fig. 6 shows an electrochemical system where the working electrode is a Cantor bar with the largest and smallest
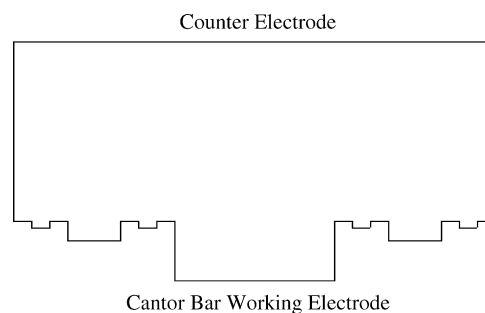

Fig. 6. The fractal electrode. The top side is the counter electrode and the bottom is a 3-stage Cantor bar working electrode. The two sides are insulating.

length scales l and ($l/27$) respectively. For this system, we have computed both the conventional secondary current distribution (with linear polarization) and the ac response of the fractal with a purely capacitive surface. Fig. 7 plots the current along the fractal boundary and it is interesting to note, though not unexpected, that the self-similarity of the fractal mirrors in the current distribution. When the smallest length in the fractal is ($l/3$) instead of ($l/27$), the corresponding current distribution is coarsened as in Fig. 8. l was taken as 5 cm.

The Nyquist ac response of the fractal was also computed and is presented in Fig. 9. This corresponds to the fractal with the smallest length ($l/27$) and a purely capacitive surface (the case relevant for CPE behavior). In the Nyquist plot, CPE manifests itself as a straight segment which makes an angle with the vertical. In Fig. 10, we observe that there is a linear portion which is restricted to the frequency range: (ω_1, ω_2). The ends of this frequency range (ω_1, ω_2) seem to nearly correspond to the largest and smallest length scales (l_1 and l_2) in the fractal through the following relations:
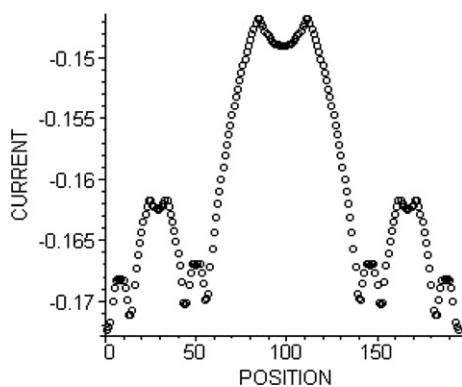

Fig. 7. The dc secondary current distribution on the fractal electrode of Fig. 6, computed using the boundary element method. Electrolyte conductivity = 0.1 S/cm and charge-transfer resistance = 250 Ω cm^2. The current is in mA.
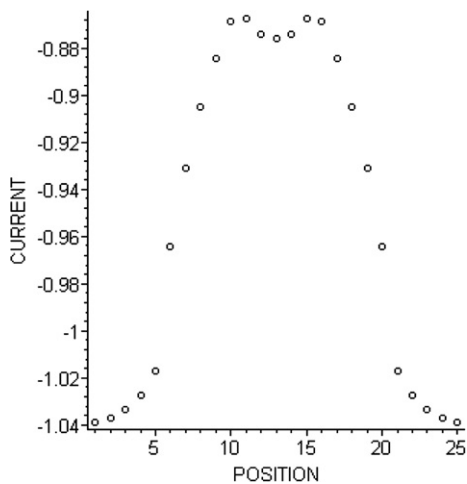

Fig. 8. Same as Fig. 7, except that the working electrode is a single-stage Cantor bar instead of the 3-stage fractal.
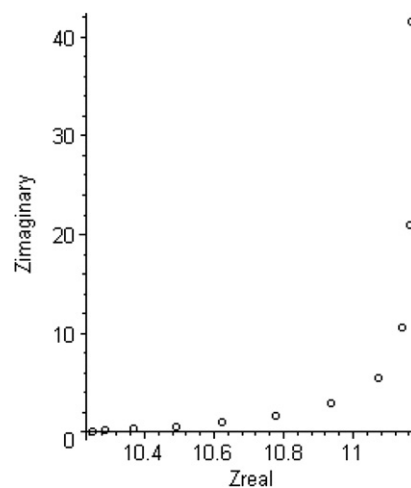

Fig. 9. Nyquist plot for the 3-stage fractal electrode with pure capacitive behavior. Electrolyte conductivity and double-layer capacity are the same as in Fig. 4 (frequency range: 1–100 kHz).
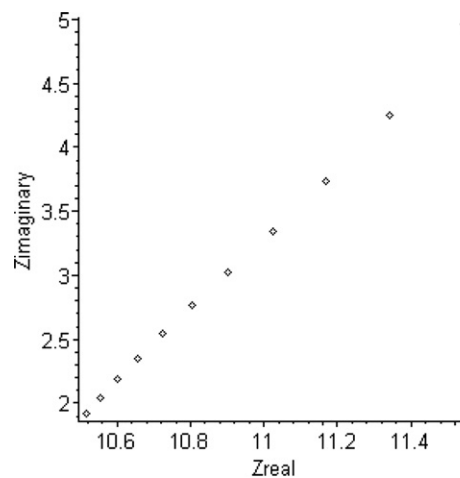

Fig. 10. Nyquist plot for the single-stage Cantor bar (frequency range: 1500–5000 Hz).

$$\omega_1 = \frac{\kappa}{l_1 C_{dl}} \qquad (23)$$

and

$$\omega_2 = \frac{\kappa}{l_2 C_{dl}} \qquad (24)$$

This leads to the interesting conclusion that the size of this linear Nyquist region depends on the length-scales l_1 and l_2 present in the electrode as well as on the electrical conductivity κ and the double-layer capacitance C_{dl}. Though it is tempting to identify this linear regime with CPE behavior, we leave this as an open question requiring more experimental and theoretical work than hitherto available.

Qualitatively, Fig. 9 is not different from the corresponding figures for the Hull cells (Fig. 4). Thus, we may expect that, whenever the working electrode has one or more parts that are not parallel to the counter electrode, it may result in a CPE-like behavior in a certain frequency range determined by the geometrical details. This in a way

explains the ubiquitous nature of CPE encountered on solid electrodes with a range of surface features. Further, Liu's transmission line model [2] for the fractal electrode predicts the CPE behavior in the entire frequency range, whereas the present work clearly shows that CPE is possible only in a limited frequency range determined by length scales present in the surface geometry, more in accord with experimental impedance data (see [5, p. 87] and references cited therein).

6. Comparison with the predictions of the TLM

In this section, we make a quantitative comparison between the predictions of the TLM and the present method based on analytic continuation implemented using the boundary element method. Fig. 11 shows a pore geometry which can interpolate between the rectangular and the saw-tooth (V-shaped groove) geometries. The prediction of the TLM for the rectangular pore is:

$$Z_{RP} = \frac{1}{\sqrt{2 * l_1 * \kappa * (j\omega * C_{dl} + 1/R_{ct})}} * \frac{1}{\tanh(\sqrt{\lambda} * L)} \tag{25}$$

where

$$\lambda = \frac{2 * (j\omega * C_{dl} + 1/R_{ct})}{l_1 * \kappa} \tag{26}$$

In Fig. 12a–d, we compare the Nyquist plots computed using Eqs. (25) and (26) with the corresponding plots computed using the present method, for finite and infinite charge-transfer resistances. One is struck by the fact that they differ by one order of magnitude both in the real and imaginary components of the impedance, with the TLM underestimating the impedance! [We are even tempted to look for a geometry-dependent scaling parameter which may connect the two.] Another difference to be noted from Fig. 12 is that the TLM predicts, at the high frequency limit, zero effective pore-solution resistance whereas the present method correctly predicts a finite value for the same quantity in addition to a different slope. To show this difference clearly, we have focused the data, in Fig. 12c and d, to the high frequency region near the origin.

The prediction of the TLM for the saw-tooth geometry is [5,14]:

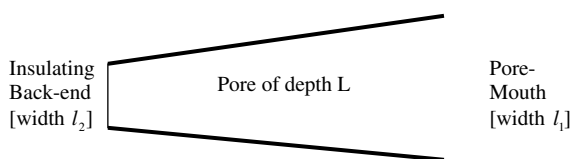$$Z_{ST} = \frac{I_0(\lambda)}{\kappa * \lambda * \tan \beta * I_1(\lambda)} \tag{27}$$

Fig. 11. Geometry of a pore with an insulating back-end. For $l_1 = l_2$ it reduces to a rectangular pore and $l_2 = 0$ results in a saw-tooth geometry. The thick lines show the working electrode. L is the pore-depth.
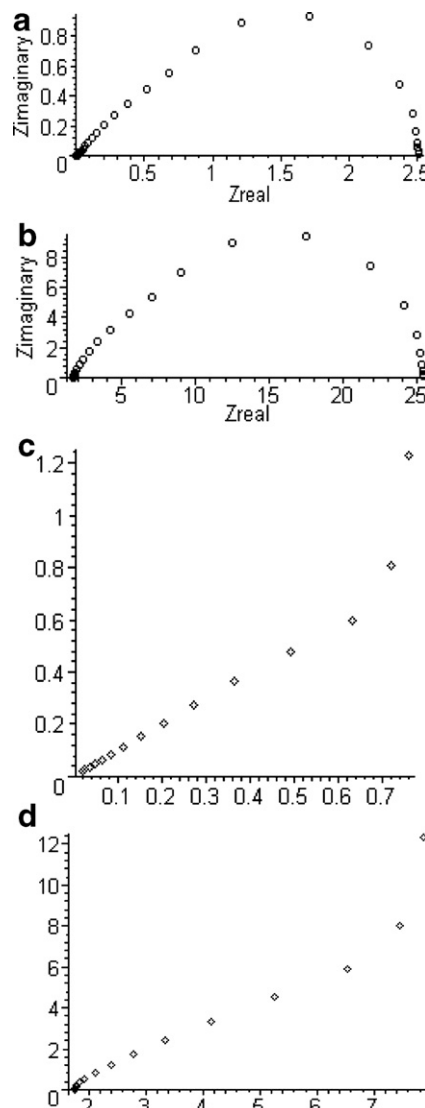

Fig. 12. Nyquist plots for a rectangular pore with the parameters: $L = 7$ cm, $l_1 = l_2 = 3$ cm, $C_{dl} = 20$ μF/cm^2, $\kappa = 0.1$ S/cm. (a) TLM with $R_{ct} = 250$ Ω cm^2, (b) analytic continuation with R_{ct} same as in (a), (c) TLM with infinite R_{ct}, (d) analytic continuation with infinite R_{ct}.

where

$$\lambda = \sqrt{4 * L * (j\omega * C_{dl} + 1/R_{ct})/(\kappa * \sin \beta)} \tag{28}$$

and 2β is the angle at the vertex of the V-shaped tooth. I_0 and I_1 are modified Bessel functions of the first kind. In Fig. 13a–d, we compare the Nyquist plots computed using Eqs. (27) and (28) with the corresponding plots computed using the present method, for finite and infinite charge-transfer resistances. One is struck by the closeness of the two predictions! However, in the high frequency limit, the differences which we noted between the predictions of the TLM and the present method for the rectangular pore continues to persist even in the case of the saw-tooth. In Fig. 13c and d, we have used a wider frequency range in order to show clearly the low frequency vertical asymptote, in contrast to Fig. 12c and d where the high frequency region was focused.
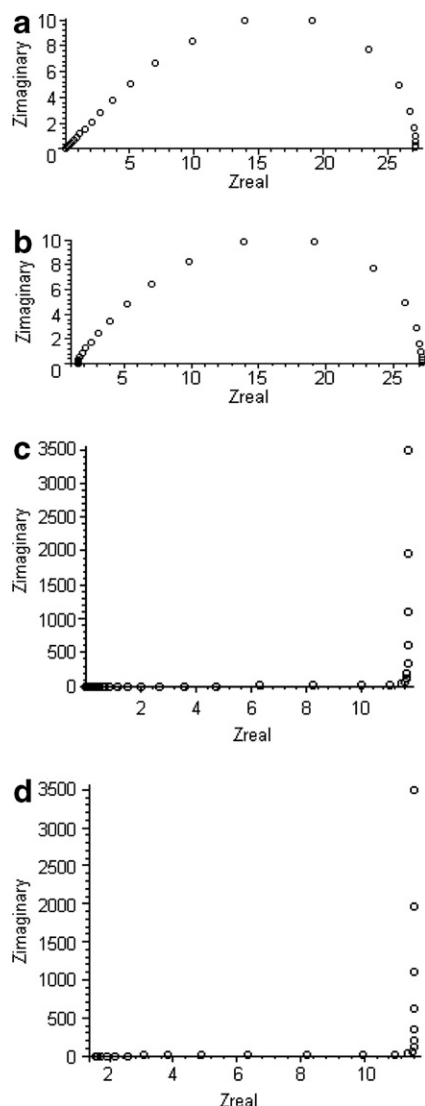
Fig. 13. Nyquist plots for a saw-tooth with the parameters: $L = 7$ cm, $l_1 = 3$ cm, $l_2 = 0$, $C_{dl} = 20$ μF/cm^2, $\kappa = 0.1$ S/cm. (a) TLM with $R_{ct} = 250\ \Omega\ cm^2$, (b) analytic continuation with R_{ct} same as in (a), (c) TLM with infinite R_{ct}, (d) analytic continuation with infinite R_{ct}.

Hence, we may conclude by saying that, while for certain geometries and model parameters the TLM may provide a good approximation, for others it may lead to significant errors at the quantitative and qualitative levels. Besides, one may not even be able to formulate a TLM for arbitrary geometries. The message is that we now have an exact method of computing the ac impedances of arbitrary electrode geometries which can provide a bench-mark for evaluating approximate methods such as TLM.

7. Analytic continuation as an approach to the constant phase element

The method of analytic continuation described in this paper provides an interesting approach to the impedance of the constant phase element:

$$Z_{CPE} = \frac{A}{(j\omega)^\alpha} \tag{29}$$

where A and α are usually treated as empirical parameters and obtained by fitting the experimental impedance data to this power law. There have been several theoretical attempts to understand this power law using pore and fractal models, distributions of relaxation times and scaling theories (see [5] and references therein). Despite much efforts by several groups, a satisfactory theory is yet to emerge to explain this power law and also to connect the CPE parameters A and α to microscopic physical material properties of the system.

Below we outline an approach to CPE based on analytic continuation and establish an experimentally verifiable connection between the CPE parameters (A and α) and the system properties such as electrolyte conductivity κ and double-layer capacity C_{dl}.

Wagner showed that secondary current distributions are controlled by the dimensionless number (named after him):

$$Wa = \kappa R_{ct}/l \tag{30}$$

where κ is the electrolyte conductivity, R_{ct} the charge-transfer resistance ($= RT/(\alpha_a + \alpha_c)F * i_0$) and l is a characteristic length scale on the electrode. i_0 is the exchange current density. West [15] studied secondary currents near the corners of V-shaped regions and showed that, in these regions, the current obeys a power law:

$$i \propto \left[\frac{(\alpha_a + \alpha_c)F * i_0}{RT\kappa}\right]^{(1-\pi/2\beta)} \tag{31}$$

where β is the vertex angle of the V-shaped groove. It is not hard to imagine a rough electrode as an assembly of sharp corners and edges with a distribution of β [This distribution may even have an underlying fractal dimension!]. Eqs. (31) and (30) predict that, near a rough electrode, the dominant contribution to the current is of the form:

$$i \propto 1/Wa^\alpha \tag{32}$$

$$\propto \left[\frac{l}{\kappa * R_{ct}}\right]^\alpha \tag{33}$$

We can now obtain the ac response of the corresponding perfectly polarisable electrode by replacing R_{ct} in Eq. (33) by $1/j\omega C_{dl}$, resulting in the CPE power law:

$$Z_{CPE} \propto (\kappa/C_{dl} \cdot l)^\alpha/(j\omega)^\alpha \tag{34}$$

Comparing Eqs. (29) and (34), we see that the CPE parameters A and α are connected to system properties by

$$A \propto (\kappa/C_{dl} \cdot l)^\alpha \tag{35}$$

and

$$\alpha = (1 - \pi/2\beta) \tag{36}$$

Interestingly, the prediction contained in Eq. (35) is supported by an experimental result reported by Scheider [3] in 1975. When he plotted, for a fixed frequency, the logarithm of the so-called "polarization capacitance" against the

logarithm of the electrolyte conductivity, straight lines were obtained. Scheider's polarization capacitance is proportional to our A parameter in Eqs. (29) and (35). Clearly, his log-log plots offer the necessary experimental support for our Eq. (35). Including the frequency dependence, the complete expression which our Eq. (34) predicts for Scheider's polarization capacitance is:

$$\text{Polarisation capacitance} \propto (\kappa/C_{dl} \cdot l)^{\alpha} \omega^{-\alpha} \qquad (37)$$

in complete agreement with Scheider's major experimental finding. The size-dependent frequency scaling implied by Eqs. (34) and (37) also provides support for the Halsey–Leibig theory [16] of the constant phase element.

8. Summary and concluding remarks

An exact alternative method is advanced in this paper, in the place of the approximate and intuitive transmission line models, for the computation of ac responses of electrochemical systems having any given geometry. This method, based on a simple and elegant analytic continuation from the secondary current distribution, was illustrated by applying it to several Hull cell geometries and a fractal geometry. A comparison with the transmission line models for the rectangular pore and the saw-tooth geometry showed that the TLM prediction for the latter agreed closely with the results of the present method and the TLM prediction for the former underestimated the impedance by one order of magnitude! The high frequency slope and intercept of the TLM was incorrect in both the cases. Lastly, an interesting alternative approach to the constant phase element was outlined using analytic continuation and its predictions were shown to be supported by experimental data.

The complex extension of the boundary element method which we have used opens up the possibility of computing the ac responses for any complicated geometry. It also provides a good bench-mark for evaluating the predictions of transmission line models. Though we restricted ourselves, in the use of BEM, to two dimensions and secondary current distributions, the method presented is more general. Extensions to 3-D and tertiary current distributions will be taken up in the future.

The complex extension of the BEM used in this paper should be clearly distinguished from the complex variable BEM developed by Hromadka et al. [17] wherein the complexity enters through the spatial variables and not through the parameters as in the present work. For the same reason our method does not have any dimensional restrictions. Hence, our method may be appropriately named complex parameter boundary element method. The two methods and their goals are essentially different.

A final remark on the existence of solutions under analytic continuation: Existence and uniqueness of solutions are important issues addressed by mathematicians. In theory we are pragmatic and go along with our methods unless there are indications to the contrary. In case of any doubt or malignancy spotted in the computed results we should of course investigate further and for such cases a Kramers–Kronig test on the computed results may be appropriate as analytic continuation, analytic functions and Kramers–Kronig relations are neatly tied to one another.

References

[1] R. de Levie, in: P. Delahay (Ed.), Advances in Electrochemistry and Electrochemical Engineering, vol. 6, Wiley, New York, 1967.
[2] S.H. Liu, Phys. Rev. Lett. 55 (1985) 529–532.
[3] W. Scheider, J. Phys. Chem. 79 (1975) 127–136.
[4] H. Keiser, K.D. Beccu, M.A. Gutjahr, Electrochim. Acta 21 (1976) 539–543.
[5] E. Barsoukov, J.R. Macdonald, Impedance Spectroscopy (Theory, Experiment and Applications), second ed., Wiley-Interscience, New Jersey, 2005 (see Chapter 2).
[6] D.D. Macdonald, Electrochim. Acta 51 (2006) 1376–1388.
[7] C.A. Brebbia, J.C.F. Telles, L.C. Wrobel, Boundary Element Techniques: Theory and Applications in Engineering, Springer, Berlin, 1984.
[8] K. Nisancioglu, in: B.E. Conway, J.O'M. Bockris, R.E. White (Eds.), Modern Aspects of Electrochemistry, vol. 23, Plenum Press, New York, 1992, pp. 149–237.
[9] N.G. Zamani, J.F. Porter, R.A. Mufti, Int. J. Numer. Methods Eng. 23 (1986) 1295–1311.
[10] V.S. Ramanan, M. Muthukumar, S. Gnanasekaran, M.J. Venkataramana Reddy, B. Emmanuel, Eng. Anal. Bound. Elem. 23 (1999) 777–786.
[11] CPSEA++: A software for cathodic protection modeling of off-shore structures, SW-1153/2003.
[12] C.A. Brebbia, S. Walker, Boundary Element Techniques in Engineering, Newns Butterworths, London, 1980.
[13] P.A. Ramachandran, Boundary Element Methods in Transport Phenomena, Elsevier, London, 1994.
[14] R. de Levie, Electrochim. Acta 10 (1965) 113–130.
[15] A.C. West, Effects of non-uniform potential and current distributions in electrochemical systems, Ph.D. Thesis, Department of Chemical Engineering, University of California, Berkeley, CA 94720, December 1989 (see Eq. (28), p. 34).
[16] T.C. Halsey, M. Leibig, Ann. Phys. 219 (1992) 109–147.
[17] T.V. Hromadka II, C. Lai, The Complex Variable Boundary Element Method in Engineering Analysis, Springer, Berlin, 1987.